



Article

Oblique and Asymmetric Klein Tunneling across Smooth NP Junctions or NPN Junctions in 8-*Pmmm* Borophene

Zhan Kong¹, Jian Li¹, Yi Zhang¹, Shu-Hui Zhang^{2,*} and Jia-Ji Zhu^{1,*}

¹ School of Science and Laboratory of Quantum Information Technology, Chongqing University of Posts and Telecommunications, Chongqing 400065, China; kongz2021@163.com (Z.K.); jianli@cqupt.edu.cn (J.L.); zhangyia@cqupt.edu.cn (Y.Z.)

² College of Mathematics and Physics, Beijing University of Chemical Technology, Beijing 100029, China

* Correspondence: shuhuizhang@mail.buct.edu.cn (S.-H.Z.); zhujj@cqupt.edu.cn (J.-J.Z.)

Abstract: The tunneling of electrons and holes in quantum structures plays a crucial role in studying the transport properties of materials and the related devices. 8-*Pmmm* borophene is a new two-dimensional Dirac material that hosts tilted Dirac cone and chiral, anisotropic massless Dirac fermions. We adopt the transfer matrix method to investigate the Klein tunneling of massless fermions across the smooth NP junctions and NPN junctions of 8-*Pmmm* borophene. Like the sharp NP junctions of 8-*Pmmm* borophene, the tilted Dirac cones induce the oblique Klein tunneling. The angle of perfect transmission to the normal incidence is 20.4°, a constant determined by the Hamiltonian of 8-*Pmmm* borophene. For the NPN junction, there are branches of the Klein tunneling in the phase diagram. We find that the asymmetric Klein tunneling is induced by the chirality and anisotropy of the carriers. Furthermore, we show the oscillation of electrical resistance related to the Klein tunneling in the NPN junctions. One may analyze the pattern of electrical resistance and verify the existence of asymmetric Klein tunneling experimentally.

Keywords: Klein tunneling; borophene; Dirac fermions



Citation: Kong, Z.; Li, J.; Zhang, Y.; Zhang, S.-H.; Zhu, J.-J. Oblique and Asymmetric Klein Tunneling across Smooth NP Junctions or NPN Junctions in 8-*Pmmm* Borophene. *Nanomaterials* **2021**, *11*, 1462. <https://doi.org/10.3390/nano11061462>

Academic Editors: Filippo Giannazzo and Eugene Kogan

Received: 10 April 2021
Accepted: 28 May 2021
Published: 31 May 2021

Publisher's Note: MDPI stays neutral with regard to jurisdictional claims in published maps and institutional affiliations.



Copyright: © 2021 by the authors. Licensee MDPI, Basel, Switzerland. This article is an open access article distributed under the terms and conditions of the Creative Commons Attribution (CC BY) license (<https://creativecommons.org/licenses/by/4.0/>).

1. Introduction

Two-dimensional (2D) materials have been the superstars for their novel properties in condensed matter physics since its first isolation of graphene in 2004 [1]. Right now, the booming 2D materials family includes not just graphene and the derivatives of graphene but also transition metal dichalcogenides (TMDs) [2–4], black phosphorus [5–8], indium selenide [9–11], stanene [12,13], and many other layered materials [14,15]. Among these 2D materials, the so-called Dirac materials host massless Dirac fermions, always in the spotlight. Carriers in 2D Dirac materials usually have chirality or pseudospin from two atomic sublattices. Together with chirality, the linear Dirac dispersion gives rise to remarkable transport properties, including the absence of backscattering [1,16,17]. Due to the suppression of backscattering, massless Dirac fermions could tunnel a single square barrier with 100% transmission probability. This surprising result has been known as Klein tunneling [16,18–21]. Klein tunneling is the basic electrical conduction mechanism through the interface between *p*-doped and *n*-doped regions. Klein tunneling's elucidation plays a key role in designing and inventing electronic devices based on 2D Dirac materials.

Recently, several 2D boron structures have been predicted and experimentally fabricated [22–25]. The 8-*Pmmm* borophene belongs to the space group *Pmmm*, which means an orthorhombic lattice has an *mmm* symmetric point group (three-mirror symmetry planes perpendicular to each other) combine with a glide plane at one of the mirror symmetry planes [22,26]. This kind of structure is the most stable symmetric phase of borophene and may be kinetically stable at ambient conditions. It revealed the tilted Dirac cone and anisotropic massless Dirac fermions by first-principles calculations [27,28]. These unique Dirac fermions attracts people to explore the various physical properties such as

strain-induced pseudomagnetic field [29], anisotropic density–density response [30–33], optical conductivity [34,35], modified Weiss oscillation [36,37], borophane and its tight-binding model [37], nonlinear optical polarization rotation [38], oblique Klein tunneling [39–41], few-layer borophane [42,43], intense light response [44,45], RKKY interaction [46,47], anomalous caustics [48], electron–phonon coupling [49], valley–contrast behaviors [50,51], Andreev reflection [52], and so on. The oblique Klein tunneling, the deviation of the perfect transmission direction to the normal direction of the interface, is induced by the anisotropic massless Dirac fermions or the tilted Dirac cone [39,53]. However, the on-site disorder or smoothing of the NP junction interface or the square potential may destroy the ideal Klein tunneling, which means the sharp interface strongly depends on high-quality fabrication state-of-the-art technology [54]. Therefore, the detailed discussion of the smooth NP junction and the tunable trapezoid potential would be helpful for the promising electronic devices based on 2D Dirac materials.

In this paper, we study the transmission properties of anisotropic and tilted massless Dirac fermions across smooth NP junctions and NPN junctions in 8-*Pmmn* borophane. Similar to the sharp NP junction, the oblique Klein tunneling retains due to the tilted Dirac cone. This conclusion does not depend on the NP junctions' doping levels as the normal Klein tunneling but depends on the junction direction. We show the angle of oblique Klein tunneling is 20.4°, a constant determined by the Hamiltonian parameters of 8-*Pmmn* borophane. For the NPN junction, there are branches of the Klein tunneling in the phase diagram. We find that the asymmetric Klein tunneling is induced by the chirality and anisotropy of the carriers [55]. The indirect consequence of the asymmetric Klein tunneling lies in the oscillation of the electrical resistance. The analysis of the pattern of the oscillation of electrical resistance would help verify the existence of asymmetric Klein tunneling experimentally.

The rest of the paper is organized as follows. In Section 2, we introduce the Hamiltonian and the energy spectrum for the 8-*Pmmn* borophane, the NP and NPN junction's potential, and present the transfer matrix method for the detailed derivation of transmissions across the junctions. In Section 3, we demonstrate perfect transmission numerically, showing that the oblique Klein tunneling in NP junctions and the asymmetric Klein tunneling in NPN junctions. Then, we calculate the electrical resistance from the Landauer formula for the NPN junction. Finally, we give a brief conclusion in Section 4.

2. Theoretical Formalism

2.1. Model

The crystal structure of 8-*Pmmn* borophane has two sublattices, as illustrated in Figure 1a by different colors. It is made of buckled triangular layers where each unit cell has eight atoms under the symmetry of space group *Pmmn* (No. 59 in [56]), the so-called 8-*Pmmn* structure. The tilted Dirac cone emerges from the hexagonal lattice formed by the inner atoms (yellow in Figure 1a) [28]. This hexagonal structure is topologically equivalent to uniaxially strained graphene, and the Hamiltonian of 8-*Pmmn* borophane around one Dirac point is given by [29,30,36,37].

$$\hat{H}_0 = v_x \sigma_x \hat{p}_x + v_y \sigma_y \hat{p}_y + v_t \mathbf{I}_{2 \times 2} \hat{p}_y \quad (1)$$

where $\hat{p}_{x,y}$ are the momentum operators, $\sigma_{x,y}$ are 2×2 Pauli matrices, and $\mathbf{I}_{2 \times 2}$ is a 2×2 unit matrix. The anisotropic velocities are $v_x = 0.86 v_F$, $v_y = 0.69 v_F$, $v_t = 0.32 v_F$, $v_F = 10^6$ m/s [29]. The energy dispersion and the corresponding wave functions of \hat{H}_0 are

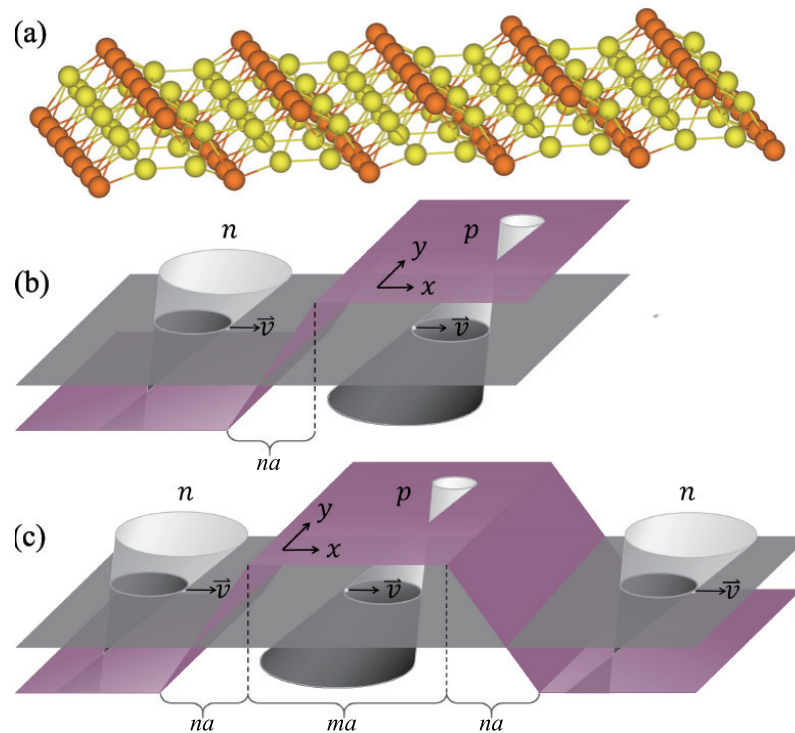


Figure 1. (a) Crystal structure of 8-*Pmmn* borophene. The unit cell of 8-*Pmmn* borophene contains two types of nonequivalent boron atoms, the ridge atoms (orange) and the inner atoms (yellow). (b) The schematic diagram of the smooth NP junction in 8-*Pmmn* borophene. Note that the true tilted Dirac cone is along *y* direction but *x* direction. (c) The schematic diagram of the smooth NPN junction in 8-*Pmmn* borophene. Here, we choose $n = 6.25$ and $m = 12.5$ for the numerical calculations.

$$E_{\lambda,\mathbf{k}} = v_t p_y + \lambda v_x \sqrt{p_x^2 + \gamma_1^2 p_y^2}, \gamma_1 = \frac{v_y}{v_x} \quad (2)$$

$$\psi_{\lambda,\mathbf{k}}(\mathbf{r}) = \frac{1}{\sqrt{2}} \left[\lambda \frac{1}{\sqrt{k_x^2 + \gamma_1^2 k_y^2}} \right] e^{i\mathbf{k}\cdot\mathbf{r}} \quad (3)$$

Here, $\lambda = \pm 1$, denoting the conduction (+1) and valence (−1) band, respectively. For 8-*Pmmn* borophene, the shape of Fermi surface for the fixing energy is elliptical with eccentricity e determined by v_x , v_y and v_t , which differs from the circular shape with radius $E_F/\hbar v_F$ of graphene. We can rewrite Equation (2) in following way [39,57]:

$$\frac{p_x^2}{a_{\lambda,E}^2} + \frac{(p_y + c_{\lambda,E})^2}{b_{\lambda,E}^2} = 1 \quad (4)$$

$$a_{\lambda,E} = \frac{v_y^2 E_{\lambda,\mathbf{k}}^2}{v_x^2 (v_y^2 - v_t^2)}, \quad b_{\lambda,E} = \frac{v_y^2 E_{\lambda,\mathbf{k}}^2}{(v_y^2 - v_t^2)^2}, \quad c_{\lambda,E} = \frac{v_t E_{\lambda,\mathbf{k}}}{(v_y^2 - v_t^2)} \quad (5)$$

The eccentricity of the Fermi surface can be determined by $e = \sqrt{v_x^2 - v_y^2 + v_t^2}/v_x$. As a direct consequence, the eccentricity is not depend on the energy and the center of ellipse is at

$$\hbar k_x = 0, \quad \hbar k_y = -\frac{v_t E_{\lambda,\mathbf{k}}}{(v_y^2 - v_t^2)} \quad (6)$$

Notice that the center of ellipse is not at the origin and it moves with increasing the Fermi levels. In a NP junction setup, the translation symmetry preserves along the *y*

axis, so the k_y is always a good quantum number. When the momentum p_y is given, the p_x in different regions of 8- $Pmmn$ borophene NP junction is

$$p_x = \pm \frac{1}{v_x} \sqrt{(E_{\lambda, \mathbf{k}} - v_t p_y)^2 - (v_y p_y)^2} \quad (7)$$

Like the graphene NP junction, one can implement a bipolar NP junction or tunable NPN-type potential barriers in 8- $Pmmn$ borophene by top/back gate voltages, and the potential function of the NP junction (as depicted in Figure 1b) has the form:

$$U_{NP}(x) = \begin{cases} V_0 & , \quad x > na/2 \\ 2V_0x/na & , \quad na/2 \leq x \leq na/2 \\ -V_0 & , \quad x < -na/2 \end{cases} \quad (8)$$

where $a = \hbar v_F/0.04$ eV is a unit length and $n > 0 \wedge n \in \mathbb{R}$. The NPN junction depicted in Figure 1c has the form

$$U_{NPN}(x) = \begin{cases} -V_0 & , \quad 3na/2 + ma < x \\ -2V_0(x - ma - na)/na & , \quad na/2 + ma \leq x \leq 3na/2 + ma \\ V_0 & , \quad na/2 < x < na/2 + ma \\ 2V_0x/na & , \quad -na/2 \leq x \leq na/2 \\ -V_0 & , \quad x < -na/2 \end{cases} \quad (9)$$

where $m > 0 \wedge m \in \mathbb{R}$. Next, we will utilize the transfer matrix method to solve the ballistic transport problem in smooth NP/NPN junctions of 8- $Pmmn$ borophene.

2.2. Transfer Matrix Method

The transfer matrix method is a powerful tool in the analysis of quantum transport of the massless fermions in 2D Dirac materials [18,58,59]. The central idea lies in that the wave function in one position can be related to those in other positions through a transfer matrix [60].

We adopt a transfer matrix method to study quantum transport in the smooth NP or NPN junction in 8- $Pmmn$ borophene. There are two different matrices in transfer matrix method: one is the transmission matrix and the other is the propagating matrix. Transmission matrix connects the electrons across an interface and the propagating matrix connects the electrons propagating over a distance in the homogeneous regions. As we can see below, the propagating matrix can be derived by the transmission matrix. We define the transmission matrix T as follows:

$$T \begin{pmatrix} A_{R_{m+1}} \\ A_{L_{m+1}} \end{pmatrix} = \begin{pmatrix} A_{R_m} \\ A_{L_m} \end{pmatrix} \quad (10)$$

where A_{R_m} (A_{L_m}) represents the right (left) traveling wave amplitude in m region. The transmission matrix connects the wave function's amplitude of two different regions. The condition of connecting amplitude coefficients between adjacent regions is the continuity of the wave functions at the interface. We can treat the smooth potential as the sum of infinite slices of junctions and figure out the wave function from the Schrödinger equation. Since the energy dispersion of 8- $Pmmn$ borophene is linear, we only need the continuity condition of the wave functions at the interface. Then, the transmission matrices T can be constructed from matrices M of each slice,

$$\begin{aligned} M(k_{m+1}, x_m) \begin{pmatrix} A_{R_{m+1}} \\ A_{L_{m+1}} \end{pmatrix} &= M(k_m, x_m) \begin{pmatrix} A_{R_m} \\ A_{L_m} \end{pmatrix} \\ M(k_m, x_m)^{-1} M(k_{m+1}, x_m) \begin{pmatrix} A_{R_{m+1}} \\ A_{L_{m+1}} \end{pmatrix} &= \begin{pmatrix} A_{R_m} \\ A_{L_m} \end{pmatrix} \\ M(k_m, x_m)^{-1} M(k_{m+1}, x_m) &= T \end{aligned}$$

Suppose that an n -doped region m is next to a p -doped region $m + 1$ and carriers go through from n -doped region to p -doped region like in Figure 2a, the wave functions at interface can be connected in the way of

$$\begin{aligned} & \frac{A_{R_{m+1}}}{\sqrt{2}} \begin{pmatrix} 1 \\ e^{i\theta_{m+1}} \end{pmatrix} e^{ik_{z,m+1}x_m + ik_y y} + \frac{A_{L_{m+1}}}{\sqrt{2}} \begin{pmatrix} 1 \\ -e^{-i\theta_{m+1}} \end{pmatrix} e^{-ik_{z,m+1}x_m + ik_y y} \\ & = \frac{A_{R_m}}{\sqrt{2}} \begin{pmatrix} 1 \\ e^{-i\theta_{m+1}} \end{pmatrix} e^{-ik_{z,m}x_m + ik_y y} + \frac{A_{L_m}}{\sqrt{2}} \begin{pmatrix} 1 \\ -e^{i\theta_{m+1}} \end{pmatrix} e^{ik_{z,m}x_m + ik_y y}. \end{aligned} \quad (11)$$

Here, we define $k_{x,m}(x)$ and θ_m as

$$k_{x,m}(x) = \frac{1}{\hbar v_x} \sqrt{(-U_m(x) + \hbar v_t k_y)^2 - (\hbar v_y k_y)^2} \quad (12)$$

$$e^{i\theta_m} = \frac{k_{x,m} + i\gamma_1 k_y}{\sqrt{k_{x,m}^2 + \gamma_1^2 k_y^2}} \quad (13)$$

where $U_m(x)$ is the doping level in m region and k_x may take positive or negative imaginary values when $(-U_m(x) + \hbar v_t k_y)^2 - (\hbar v_y k_y)^2 < 0$. The phase $e^{i\theta_m}$ in Equation (11) is defined as the wave function phase difference between the two sublattices. The sign of the k_x defines the propagating direction of the carriers. Without loss of generality, we can take only positive imaginary value for the transmission matrix, which means the positive propagating direction of electrons is defined on right-going state. Here, the potential profile $U_m(x)$ in adjacent regions within NP junction is linear but not rectangular; we treat the potential as a series of step potential to solve the tunneling problems by the transmission matrices. For convenience, we choose $a = \hbar v_F / 0.04$ eV to be the length unit and 0.01 eV to be the energy unit, where 0.04 eV is the maximum of the doping level.

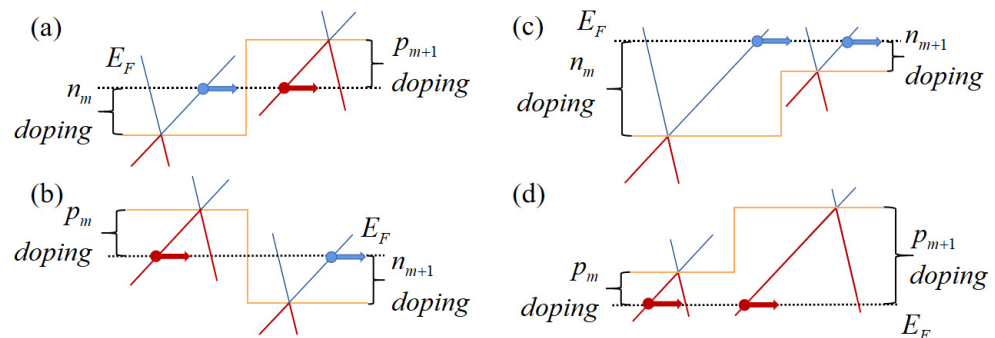


Figure 2. Potential profile of (a) NP junction, (b) PN junction, (c) NN junction, and (d) PP junction in each slice of the junctions.

Then, we rewrite the Equation (11) to construct the transmission matrices

$$\begin{aligned} & \begin{pmatrix} e^{-ik_{x,m+1}x_m} & e^{ik_{x,m+1}x_m} \\ e^{-i\theta_{m+1}} e^{-ik_{x,m+1}x_m} & -e^{i\theta_{m+1}} e^{ik_{x,m+1}x_m} \end{pmatrix} \begin{pmatrix} A_{R_{m+1}} \\ A_{L_{m+1}} \end{pmatrix} \\ & = \begin{pmatrix} e^{ik_{x,m}x_m} & e^{-ik_{x,m}x_m} \\ e^{i\theta_m} e^{ik_{x,m}x_m} & -e^{-i\theta_m} e^{-ik_{x,m}x_m} \end{pmatrix} \begin{pmatrix} A_{R_m} \\ A_{L_m} \end{pmatrix}. \end{aligned}$$

Therefore, the transmission matrix between m and $m + 1$ region is

$$T_{m,m+1}^{n \rightarrow p} = \begin{pmatrix} e^{ik_{x,m}x_m} & e^{-ik_{x,m}x_m} \\ e^{i\theta_m} e^{ik_{x,m}x_m} & -e^{-i\theta_m} e^{-ik_{x,m}x_m} \end{pmatrix}^{-1} \begin{pmatrix} e^{-ik_{x,m+1}x_m} & e^{ik_{x,m+1}x_m} \\ e^{-i\theta_{m+1}} e^{-ik_{x,m+1}x_m} & -e^{i\theta_{m+1}} e^{ik_{x,m+1}x_m} \end{pmatrix} \quad (14)$$

while the transmission matrices of the carriers going through from p -doped region m to n -doped region $m + 1$ and between two n -doped or p -doped region (shown in Figure 2) are

$$T_{m,m+1}^{p \rightarrow n} = \begin{pmatrix} e^{-ik_{x,m}x_m} & e^{ik_{x,m}x_m} \\ e^{-i\theta_m} e^{-ik_{x,m}x_m} & -e^{i\theta_m} e^{ik_{x,m}x_m} \end{pmatrix}^{-1} \begin{pmatrix} e^{ik_{x,m+1}x_m} & e^{-ik_{x,m+1}x_m} \\ e^{i\theta_{m+1}} e^{ik_{x,m+1}x_m} & -e^{-i\theta_{m+1}} e^{-ik_{x,m+1}x_m} \end{pmatrix} \quad (15)$$

$$T_{m,m+1}^{n \rightarrow n} = \begin{pmatrix} e^{ik_{x,m}x_m} & e^{-ik_{x,m}x_m} \\ e^{i\theta_m} e^{ik_{x,m}x_m} & -e^{-i\theta_m} e^{-ik_{x,m}x_m} \end{pmatrix}^{-1} \begin{pmatrix} e^{ik_{x,m+1}x_m} & e^{-ik_{x,m+1}x_m} \\ e^{i\theta_{m+1}} e^{ik_{x,m+1}x_m} & -e^{-i\theta_{m+1}} e^{-ik_{x,m+1}x_m} \end{pmatrix} \quad (16)$$

$$T_{m,m+1}^{p \rightarrow p} = \begin{pmatrix} e^{-ik_{x,m}x_m} & e^{ik_{x,m}x_m} \\ e^{-i\theta_m} e^{-ik_{x,m}x_m} & -e^{i\theta_m} e^{ik_{x,m}x_m} \end{pmatrix}^{-1} \begin{pmatrix} e^{-ik_{x,m+1}x_m} & e^{ik_{x,m+1}x_m} \\ e^{-i\theta_{m+1}} e^{-ik_{x,m+1}x_m} & -e^{i\theta_{m+1}} e^{ik_{x,m+1}x_m} \end{pmatrix} \quad (17)$$

For the case of NPN junction, a trapezoidal potential profile as in Figure 1c, we can also treat the trapezoidal potential into infinite slices of connected step potentials. The transmission matrices define at the interface between each step potentials. Multiplying all the transmission matrices would give the propagation matrices,

$$T_{all} = T_{0,1}^{n \rightarrow n} T_{1,2}^{n \rightarrow n} \cdots T_{k-1,k}^{n \rightarrow n} T_{k,k+1}^{n \rightarrow p} T_{k+1,k+2}^{p \rightarrow p} \cdots \times T_{k'-1,k'}^{p \rightarrow p} T_{k',k'+1}^{p \rightarrow p} \cdots T_{k''-1,k''}^{p \rightarrow p} T_{k'',k''+1}^{p \rightarrow n} T_{k''+1,k''+2}^{n \rightarrow n} \cdots T_{m-2,m-1}^{n \rightarrow n} T_{m-1,m}^{n \rightarrow n} \quad (18)$$

Then, we reach the formula

$$T_{all} \begin{pmatrix} A_{R_m} \\ A_{L_m} \end{pmatrix} = \begin{pmatrix} A_{R_0} \\ A_{L_0} \end{pmatrix} \quad (19)$$

When incident electrons go from the leftmost side of the NPN junction to the rightmost side, there are no reflection states in the rightmost side, i.e., $A_{L_m} = 0$. We can connect the amplitude of incident states to the amplitude of reflection states

$$\begin{pmatrix} T_{11} & T_{12} \\ T_{21} & T_{22} \end{pmatrix} \begin{pmatrix} A_{R_m} \\ 0 \end{pmatrix} = \begin{pmatrix} A_{R_0} \\ A_{L_0} \end{pmatrix} \\ \frac{A_{R_m}}{A_{R_0}} = \frac{1}{T_{11}}$$

Finally, the transmission probability is $T = |t|^2 = |A_{R_m}/A_{R_0}|^2 = |1/T_{11}|^2$.

There is a trick in constructing the propagation matrices from the transmission matrices. As shown in Figure 3, the incident states at the left-hand side of the junction have a different Fermi surface from the transmitted states at the right-hand side in the NP junction. Suppose the NP junction is sharp. The good quantum number k_y should be restricted between the top dotted green line and the middle dotted green line, since the incident states and the transmitted states are propagating only in this scenario. While supposing the NP junction is smooth, the Fermi surface in the region of varying potential would shrink to the Dirac point, and the $E_{\lambda,k}$, $a_{\lambda,E}$, $b_{\lambda,E}$, and $c_{\lambda,E}$ from Equation (5) reduce to zero as well. Therefore, k_x vanishes to diverge the transmission matrices when the carriers approaching the NP junction center. However, we could play a trick by properly segmenting the region of varying potential and jumping the diverging point. The trick lies in the fact that the carriers would not experience any singularity when going through an infinitesimal interval around the diverging point. For instance, the transmission matrix at the Dirac point cannot be well defined with incident states $k_y = 0$, whereas the carriers are well-defined decay states at the Dirac point. We can ignore

the decay states of the carriers going through infinitesimal intervals around the Dirac point, and it would eliminate any possible ambiguity.

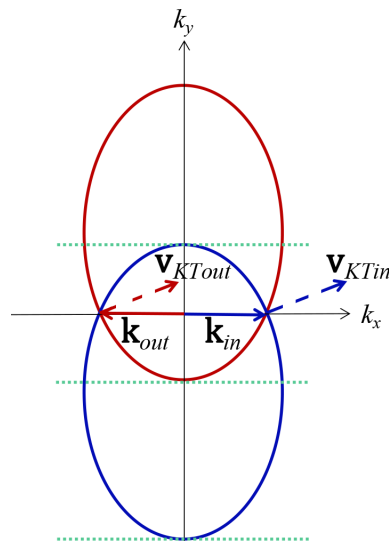


Figure 3. Fermi surface at different doped regions $\pm\varepsilon_{doping}$. The blue (red) ellipse represents the electron (hole) Fermi surface in n -doped (p -doped) region. The solid vectors \mathbf{k}_{in} (blue) and \mathbf{k}_{out} (red) are the wave vector of incident carriers and transmitted carriers, respectively. The dashed vectors \mathbf{v}_{KTin} (blue) and \mathbf{v}_{KTout} (red) are the group velocity of incident carriers and transmitted carriers, respectively. The green dotted lines indicate the values of the good quantum number k_y posed restrictions for the NP junction and the NPN junction.

3. Results and Discussions

In this section, we present the numerical results for the transmission probability and electrical conduction of the massless Dirac fermions across the borophene NP junction and NPN junction.

3.1. The Oblique Klein Tunneling in Smooth NP Junctions

Various smooth NP junctions with fixing n/p doping level but different slopes are depicted in Figure 4a. We set the length of the varying region in different NP junctions as $6.25a$, $12.5a$, $25a$, and $50a$, respectively, where $a = \hbar v_F / 0.04 \text{ eV}$, and plot the angular transmission probability for different NP junctions. As shown in Figure 4b, the sharper the NP junction is, the wider the angular transmission probability spans. This phenomenon is caused by the decay states in the varying region and is similar to the graphene smooth NP junction. In the varying region, $(-U_m(x) + \hbar v_t k_y)^2 - (\hbar v_y k_y)^2 < 0$, so that the propagating states degenerate to the decaying states when the carriers gradually approach the junction's center. Therefore, the transmission probability increases with increasing the slope of potential in the varying region. If we take $k_y = 0$, i.e., the normal incident case, we can see the perfect transmission, the Klein tunneling.

Figure 5 shows that the angular transmission amplitude of the k vector is different from the one of group velocity. The actual incident angle across the junction is based on the group velocity of carriers. The actual angular transmission probability for group velocity shown in Figure 5 indicates a rotation of the Klein tunneling, the oblique Klein tunneling. It means that the perfect transmission does not occur in the normal incident but with a nonzero angle θ_K .

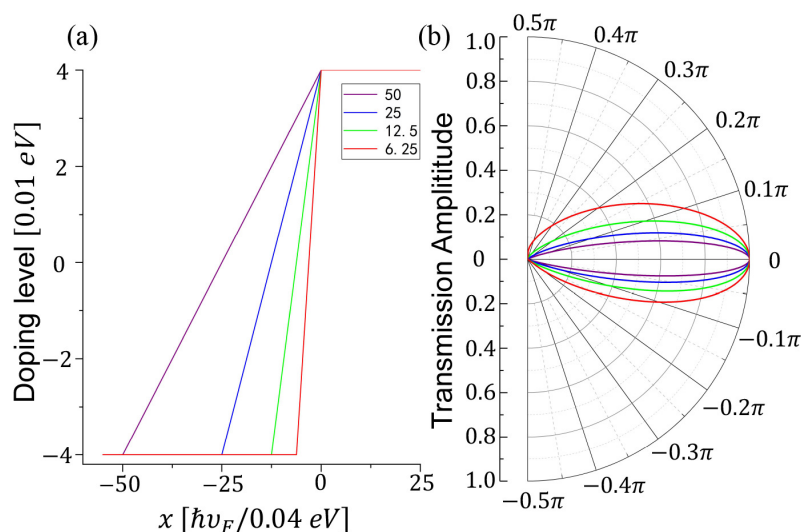


Figure 4. (a) Potential profile of smooth NP junctions and (b) the angular behavior of the transmission probability for different NP junctions corresponding to different colors at (a).

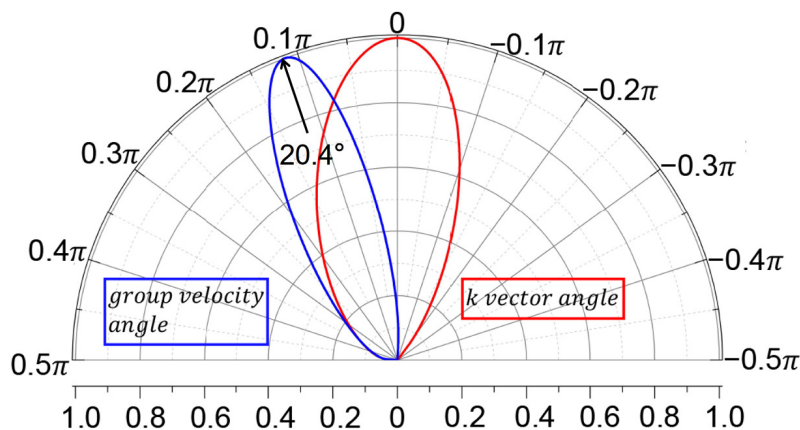


Figure 5. Angular transmission amplitude for k vector (red) and for group velocity (blue). The doping level is 0.04 eV and the length of varying region is 6.25 a .

The value of θ_K can be determined from the elliptical Fermi surface of 8- $Pmmn$ borophene. The angle for the group velocity is $\theta_v = \arctan[v_y(\epsilon, k_y)/v_x(\epsilon, k_y)]$, where $v_y(\epsilon, k_y)$ and $v_x(\epsilon, k_y)$ can be obtained by

$$v_x(\epsilon, k_y) = \frac{\partial E_{\lambda, \mathbf{k}}}{\hbar \partial k_x} = \frac{\lambda k_x v_x}{\sqrt{k_x^2 + \gamma_1^2 k_y^2}} \tag{20}$$

$$v_y(\epsilon, k_y) = \frac{\partial E_{\lambda, \mathbf{k}}}{\hbar \partial k_y} = v_t + \frac{\lambda \gamma_1^2 k_y v_x}{\sqrt{k_x^2 + \gamma_1^2 k_y^2}} \tag{21}$$

Combined with above equations and let $k_y = 0$, we can find the angle of Klein tunneling for group velocity,

$$\theta_K = \arctan\left(\frac{v_t}{v_x}\right) \approx 20.4^\circ \tag{22}$$

This oblique Klein tunneling can also be found in sharp NP junctions of 8- $Pmmn$ borophene [39,53].

3.2. The Asymmetric Klein Tunneling in the Smooth NPN Junctions

The NPN junction, as shown in the Figure 1c, can be seen as a trapezoid potential barrier. We set the length of the varying regions as $6.25 a$ and the length of the flat potential barrier as $12.5 a$.

In Figure 6, we plot the transmission probability depending on different doping levels and k_y . Note that n - and p -regions have the same absolute value of doping level. We can see the Klein tunneling in several branches. The number of branches increases by lifting the doping level, which could also be observed in the graphene NPN junctions [16,18]. We can see the Klein tunneling is asymmetric. The asymmetric Klein tunneling results from the carriers' chirality and anisotropy [61]. It is not surprising to see it here because the carriers of $8-Pmmn$ have both chirality and anisotropy.

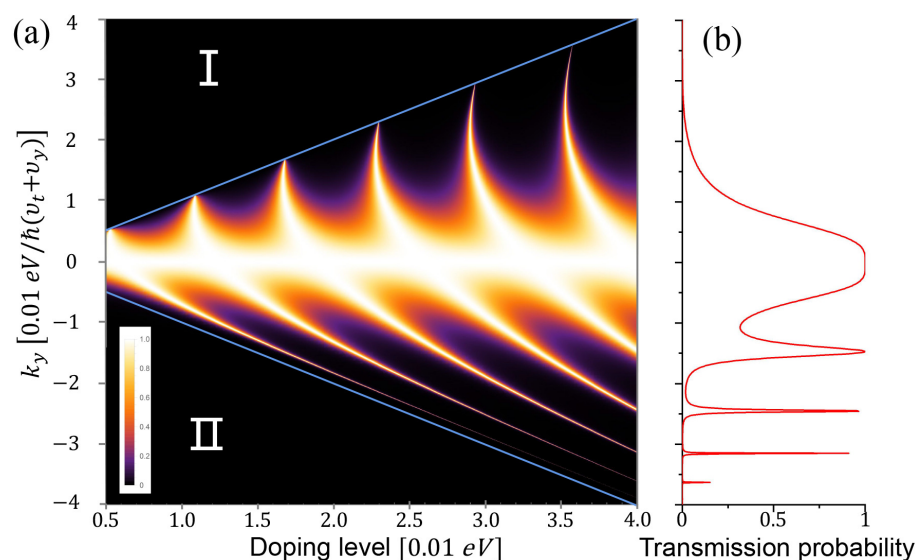


Figure 6. (a) Transmission probability versus the doping level and the k_y in NPN junction. Blue lines denote the forbidden zone, where transmission probability vanishes, and there are only the decaying states in the p -doped region. (b) The transmission probability depending on k_y when the doping level is $4 \times 0.01 eV$.

The blue lines in Figure 6a denote the forbidden zones, where the transmission probability vanishes. The equation of the boundary of the forbidden zone is $k_y = \pm \varepsilon_{doping}/\hbar(v_t + v_y)$. There are two types of the forbidden zone: (I) the no-incident zone and (II) the vanishing transmitted zone. In the no-incident zone $k_y \geq \varepsilon_{doping}/\hbar(v_t + v_y)$, there is no incident states since the parameters k_y and doping level is beyond the Dirac cone; in the vanishing transmitted zone $k_y \leq -\varepsilon_{doping}/\hbar(v_t + v_y)$, the transmitted carriers severely decay in the region of barrier.

Next, we fix the bottom edge and the height of the trapezoid potential (NPN junction) and plot the transmission probability versus the potential's top edge. When the top edge's length varies from 0 to the bottom edge's length, the NPN junction experiences a change from triangle potential to trapezoid potential and finally to a square potential. We can see from Figure 7, the number of branches increases with increasing the top edge's length. It is somehow counterintuitive that the square potential favors Klein tunneling more than the triangle potential. The reason is that the carriers would have more chances to degenerate to decaying states when incident into a slope of potential, in fact, a smooth NP junction.

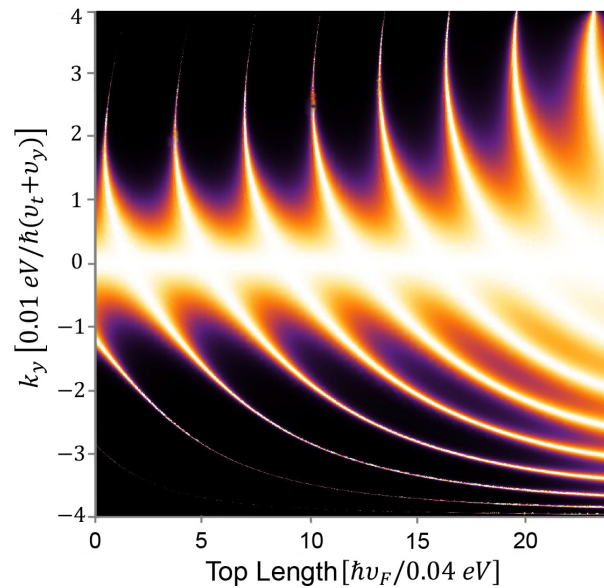


Figure 7. Transmission probability depends on top edge of the trapezoid potentials. The top edge varies from 0 to $24 a$ and the bottom edge is fixed as $25 a$. The height of the trapezoid potentials or the absolute value of n/p doping level is fixed as $0.04 eV$.

3.3. The Electrical Resistance of the Smooth NPN Junctions

One can create the NPN junction by implementing a design with two electrostatic gates, a global back gate and a local top gate. A back voltage applied to the back gate could tune the carrier density in the borophene sheet, whereas a top voltage applied to the top gate could tune the density only in the narrow strip below the gate. These two gates can be controlled independently [62].

To clarify the effect of the Klein tunneling on the transport property, here, we discuss the electrical conduction of the NPN junction in $8-Pmmn$ borophene. In the ballistic regime, we apply the Landauer–Buttiker formula $G = 2e^2 MT/h$ to calculate the electrical conductance [63]. In our setup, the Landauer formula can be written as [64]

$$G_{fet} = \frac{4e^2}{h} \sum_{ch.} T_{ch} \approx \frac{4e^2}{h} \int_{k_{y \min}}^{k_{y \max}} \frac{dk_y}{2\pi/W} T(k_y) \quad (23)$$

where $k_{y \max} = \varepsilon_{doping}/\hbar(v_t + v_y)$ and $k_{y \min} = \varepsilon_{doping}/\hbar(v_t - v_y)$.

We choose the width of the junction $W = 10 \mu m$ and calculate the electrical resistance by the Landauer formula. To reveal the link of the resistance with the Klein tunneling, we plot the transmission probability versus the doping level in Figure 8a and the resistance depending on doping levels in Figure 8b. We can see the resistance oscillation when increasing the doping level from 0 to $0.08 eV$. The oscillation pattern indicates the effect of the Klein tunneling. When the doping level varies from 0 to $-0.08 eV$, the NPN junction becomes a NNN junction so that the curves of resistance are flat in the negative doping regime.

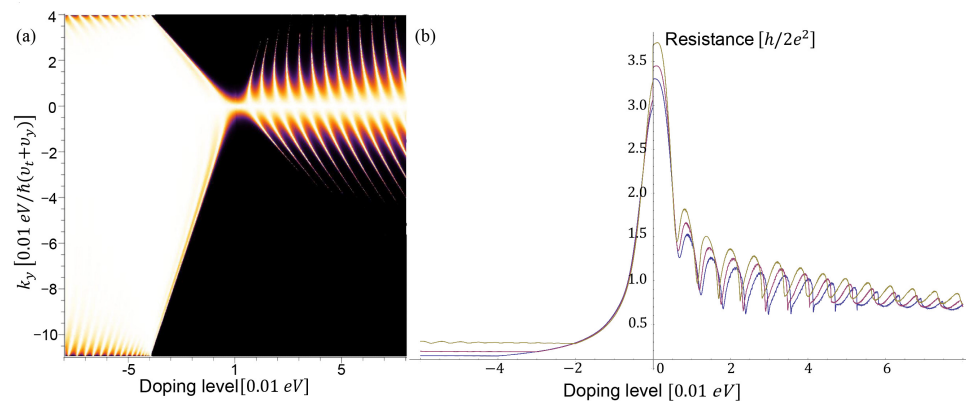


Figure 8. (a) Transmission probability depends on k_y and the height of the trapezoid potentials (doping levels of the NPN junctions). The top edge's length is $12.5 a$ and the bottom edge's length is $25 a$. The doping level of n -doped region (outside the NPN junction) is set -0.04 eV . (b) The electrical resistance of the NPN junction depending on the doping level.

4. Conclusions

This work investigates the transport properties of massless fermions in the smooth $8-Pmmn$ borophene NP and NPN junctions by the transfer matrix method. Compare with the sharp junction, the smooth NP junction also shows that the oblique Klein tunneling induced by the tilted Dirac cones. We can calculate from the parameters of the Hamiltonian that the angle of oblique Klein tunneling is 20.4° . We also show the branches of the NPN tunneling in the phase diagram, which indicates the asymmetric Klein tunneling. The physical origin of the asymmetric Klein tunneling lies in the chirality and anisotropy of the carriers, and we can verify the asymmetric Klein tunneling experimentally by analyzing the pattern of the electrical resistance oscillation. For the oblique Klein tunneling, we have discussed the experimental feasibility in detail in our previous study [39]. The present numerical demonstration in smooth junctions proves the effectiveness of our previous discussion and favors the observation in future experiments.

Author Contributions: Conceptualization, J.-J.Z. and S.-H.Z.; investigation, Z.K., S.-H.Z., and J.-J.Z.; writing—original draft preparation, Z.K.; writing—review and editing, all authors; visualization, Z.K.; supervision, J.-J.Z. and S.-H.Z.; funding acquisition, J.-J.Z., J.L., and Y.Z. All authors have read and agreed to the published version of the manuscript.

Funding: This work was supported by the Scientific Research Program from Science and Technology Bureau of Chongqing City (Grant No. cstc2020jcyj-msxm0925, cstc2020jcyj-msxmX0810), the Science and Technology Research Program of Chongqing Municipal Education Commission (Grant No. KJQN202000639), and the key technology innovations project to industries of Chongqing (cstc2016zdcy-ztzx0067).

Data Availability Statement: The study did not report any data.

Conflicts of Interest: The authors declare no conflict of interest.

References

1. Neto, A.H.C.; Guinea, F.; Peres, N.M.R.; Novoselov, K.S.; Geim, A.K. The electronic properties of graphene. *Rev. Mod. Phys.* **2009**, *81*, 109–162. [[CrossRef](#)]
2. Xiao, D.; Liu, G.-U.; Feng, W.-A.; Xu, X.-I.; Yao, W. Coupled Spin and Valley Physics in Monolayers of MoS₂ and Other Group-VI Dichalcogenides. *Phys. Rev. Lett.* **2012**, *108*, 196802. [[CrossRef](#)]
3. Wang, Q.-I.; Kalantar-Zadeh, K.; Kis, A.; Coleman, J.N.; Strano, M.S. Electronics and optoelectronics of two-dimensional transition metal dichalcogenides. *Nat. Nanotechnol.* **2012**, *7*, 699–712. [[CrossRef](#)]
4. Zhang, K.-E.; Zhang, T.-I.; Cheng, G.-U.; Li, T.-I.; Wang, S.; Wei, W.; Zhou, X.-I.; Yu, W.-E.; Sun, Y.; Wang, P.; et al. Interlayer Transition and Infrared Photodetection in Atomically Thin Type-II MoTe₂/MoS₂ van der Waals Heterostructures. *ACS Nano* **2016**, *10*, 3852–3858. [[CrossRef](#)]

5. Du, Y.-L.; Ouyang, C.-Y.; Shi, S.-Q.; Lei, M.-S. Electronic Ab initio studies on atomic and electronic structures of black phosphorus. *J. Appl. Phys.* **2010**, *107*, 093718. [[CrossRef](#)]
6. Li, L.-K.; Kim, J.; Jin, C.-H.; Ye, G.-J.; Qiu, D.Y.; Felipe, H.; Shi, Z.-W.; Chen, L.; Zhang, Z.-C.; Yang, F.-Y.; et al. Direct observation of the layer-dependent electronic structure in phosphorene. *Nat. Nanotechnol.* **2017**, *12*, 21–25. [[CrossRef](#)] [[PubMed](#)]
7. Li, L.-K.; Yang, F.-Y.; Ye, G.-J.; Zhang, Z.-C.; Zhu, Z.-W.; Lou, W.-K.; Zhou, X.-Y.; Li, L.; Watanabe, K.; Taniguchi, T.; et al. Quantum Hall effect in black phosphorus two-dimensional electron system. *Nat. Nanotechnol.* **2016**, *11*, 593–597.
8. Zhou, X.-Y.; Lou, W.-K.; Zhai, F.; Chang, K. Anomalous magneto-optical response of black phosphorus thin films. *Phys. Rev. B* **2015**, *92*, 165405. [[CrossRef](#)]
9. Tamalampudi, S.R.; Lu, Y.-Y.; Sankar, R.K.U.R.; Liao, C.-D.; Cheng, K.M.B.C.; Chou, F.-C.; Chen, Y.-T. High Performance and Bendable Few-Layered InSe Photodetectors with Broad Spectral Response. *Nano Lett.* **2014**, *14*, 2800–2806. [[CrossRef](#)] [[PubMed](#)]
10. Brotons-Gisbert, M.; Andres-Penares, D.; Suh, J.; Hidalgo, F.; Abargues, R.; Rodríguez-Cantó, P.J.; Segura, A.; Cros, A.; Tobias, G.; Canadell, E.; et al. Nanotexturing To Enhance Photoluminescent Response of Atomically Thin Indium Selenide with Highly Tunable Band Gap. *Nano Lett.* **2016**, *16*, 3221–3229. [[CrossRef](#)]
11. Bandurin, D.A.; Tyurnina, A.V.; Yu, G.L.; Mishchenko, A.; Zólyomi, V.; Morozov, S.V.; Kumar, R.K.; Gorbachev, R.V.; Kudrynskiy, Z.R.; Pezzini, S.; et al. High electron mobility, quantum Hall effect and anomalous optical response in atomically thin InSe. *Nat. Nanotechnol.* **2017**, *12*, 223–227. [[CrossRef](#)]
12. Xu, Y.; Yan, B.-H.; Zhang, H.-J.; Wang, J.; Xu, G.; Tang, P.-Z.; Duan, W.-H.; Zhang, S.-C. Large-Gap Quantum Spin Hall Insulators in Tin Films. *Phys. Rev. Lett.* **2013**, *111*, 136804. [[CrossRef](#)] [[PubMed](#)]
13. Zhu, F.-F.; Chen, W.-J.; Xu, Y.; Gao, C.-L.; Guan, D.-D.; Liu, C.-H.; Qian, D.; Zhang, S.-C.; Jia, J.-F. Epitaxial growth of two-dimensional stanene. *Nat. Mater.* **2015**, *14*, 1020–1025. [[CrossRef](#)] [[PubMed](#)]
14. Novoselov, K.S.; Mishchenko, A.; Carvalho, A.; Neto, A.H.C. 2D materials and van der Waals heterostructures. *Science* **2016**, *353*, 9493. [[CrossRef](#)] [[PubMed](#)]
15. Schaibley, J.R.; Yu, H.-Y.; Clark, G.; Rivera, P.; Ross, J.S.; Seyler, K.L.; Yao, W.; Xu, X.-D. Valleytronics in 2D materials. *Nat. Rev. Mater.* **2016**, *1*, 1–15. [[CrossRef](#)]
16. Beenakker, C.W.J. Colloquium: Andreev reflection and Klein tunneling in graphene. *Rev. Mod. Phys.* **2008**, *80*, 1337–1354. [[CrossRef](#)]
17. Wu, Z.-H.; Peeters, F.M.; Chang, K. Electron tunneling through double magnetic barriers on the surface of a topological insulator. *Phys. Rev. B* **2010**, *82*, 115211. [[CrossRef](#)]
18. Bai, C.-X.; Zhang, X.-X. Klein paradox and resonant tunneling in a graphene superlattice. *Phys. Rev. B* **2007**, *76*, 075430. [[CrossRef](#)]
19. Pereira, J.M., Jr.; Peeters, F.M.; Chaves, A.; Farias, G.A. Klein tunneling in single and multiple barriers in graphene. *Semicond. Sci. Technol.* **2010**, *25*, 033002. [[CrossRef](#)]
20. Oh, H.; Coh, S.; Son, Y.-W.; Cohen, M.L. Inhibiting Klein Tunneling in a Graphene p-n Junction without an External Magnetic Field. *Phys. Rev. Lett.* **2016**, *117*, 016804. [[CrossRef](#)]
21. Cheianov, V.V.; Fal'ko, V.I. Selective transmission of Dirac electrons and ballistic magnetoresistance of n-p junctions in graphene. *Phys. Rev. B* **2006**, *74*, 041403. [[CrossRef](#)]
22. Zhou, X.-F.; Dong, X.; Oganov, A.R.; Zhu, Q.; Tian, Y.-J.; Wang, H.-T. Semimetallic Two-Dimensional Boron Allotrope with Massless Dirac Fermions. *Phys. Rev. Lett.* **2014**, *112*, 085502. [[CrossRef](#)]
23. Mannix, A.J.; Zhou, X.-F.; Kiraly, B.; Wood, J.D.; Alducin, D.; Myers, B.D.; Liu, X.-L.; Fisher, B.L.; Santiago, U.; Guest, J.R.; et al. Synthesis of borophenes: Anisotropic, two-dimensional boron polymorphs. *Science* **2015**, *350*, 1513–1516. [[CrossRef](#)]
24. Jiao, Y.-L.; Ma, F.-X.; Bell, J.; Bilic, A.; Du, A.-J. Two-Dimensional Boron Hydride Sheets: High Stability, Massless Dirac Fermions, and Excellent Mechanical Properties. *Angew. Chem.* **2016**, *128*, 10448–10451. [[CrossRef](#)]
25. Kunstmann, J.; Quandt, A. Broad boron sheets and boron nanotubes: An ab initio study of structural, electronic, and mechanical properties. *Phys. Rev. B* **2006**, *74*, 035413. [[CrossRef](#)]
26. Dresselhaus, M.S.; Dresselhaus, G.; Jorio, A. *Group Theory: Application to the Physics of Condensed Matter*; Springer: Berlin/Heidelberg, Germany, 2008; pp. 190–191.
27. Feng, B.-J.; Sugino, O.; Liu, R.-Y.; Zhang, J.; Yukawa, R.; Kawamura, M.; Iimori, T.; Kim, H.-W.; Hasegawa, Y.; Li, H.; et al. Dirac Fermions in Borophene. *Phys. Rev. Lett.* **2017**, *118*, 096401. [[CrossRef](#)]
28. Lopez-Bezanilla, A.; Littlewood, P.B. Electronic properties of 8-*Pmmn* borophene. *Phys. Rev. B* **2016**, *93*, 241405. [[CrossRef](#)]
29. Zabolotskiy, A.D.; Lozovik, Y.E. Strain-induced pseudomagnetic field in the Dirac semimetal borophene. *Phys. Rev. B* **2016**, *94*, 165403. [[CrossRef](#)]
30. Sadhukhan, K.; Agarwal, A. Anisotropic plasmons, Friedel oscillations, and screening in 8-*Pmmn* borophene. *Phys. Rev. B* **2017**, *96*, 035410. [[CrossRef](#)]
31. Jalali-Mola, Z.; Jafari, S.A. Tilt-induced kink in the plasmon dispersion of two-dimensional Dirac electrons. *Phys. Rev. B* **2018**, *98*, 195415. [[CrossRef](#)]
32. Jalali-Mola, Z.; Jafari, S.A. Kinked plasmon dispersion in borophene-borophene and borophene-graphene double layers. *Phys. Rev. B* **2018**, *98*, 235430. [[CrossRef](#)]
33. Lian, C.; Hu, S.-Q.; Zhang, J.; Cheng, C.; Yuan, Z.; Gao, S.-W.; Meng, S. Integrated Plasmonics: Broadband Dirac Plasmons in Borophene. *Phys. Rev. Lett.* **2020**, *125*, 116802. [[CrossRef](#)] [[PubMed](#)]

34. Verma, S.; Mawrie, A.; Ghosh, T.K. Effect of electron-hole asymmetry on optical conductivity in 8-*Pmmn* borophene. *Phys. Rev. B* **2017**, *96*, 155418. [[CrossRef](#)]
35. Mojarro, M.A.; Carrillo-Bastos, R.; Maytorena, J.A. Optical properties of massive anisotropic tilted Dirac systems. *Phys. Rev. B* **2021**, *103*, 165415. [[CrossRef](#)]
36. Islam, S.K.F.; Jayannavar, A.M. Signature of tilted Dirac cones in Weiss oscillations of 8-*Pmmn* borophene. *Phys. Rev. B* **2017**, *96*, 235405. [[CrossRef](#)]
37. Nakhaee, M.; Ketabi, S.A.; Peeters, F.M. Tight-binding model for borophene and borophane. *Phys. Rev. B* **2018**, *97*, 125424. [[CrossRef](#)]
38. Singh, A.; Ghosh, S.; Agarwal, A. Nonlinear and anisotropic polarization rotation in two-dimensional Dirac materials. *Phys. Rev. B* **2018**, *97*, 205420. [[CrossRef](#)]
39. Zhang, S.-H.; Yang, W. Oblique Klein tunneling in 8-*Pmmn* borophene $p - n$ junctions. *Phys. Rev. B* **2018**, *97*, 235440. [[CrossRef](#)]
40. Zhou, X.-F. Valley-dependent electron retroreflection and anomalous Klein tunneling in an 8-*pmm* borophene-based $n - p - n$ junction. *Phys. Rev. B* **2019**, *100*, 195139. [[CrossRef](#)]
41. Zhou, X.-F. Valley splitting and anomalous Klein tunneling in borophane-based $n - p$ and $n - p - n$ junctions. *Phys. Lett. A* **2020**, *384*, 126612. [[CrossRef](#)]
42. Zhong, H.-X.; Huang, K.-X.; Yu, G.-D.; Yuan, S.-J. Electronic and mechanical properties of few-layer borophene. *Phys. Rev. B* **2018**, *98*, 054104. [[CrossRef](#)]
43. Nakhaee, M.; Ketabi, S.A.; Peeters, F.M. Dirac nodal line in bilayer borophene: Tight-binding model and low-energy effective Hamiltonian. *Phys. Rev. B* **2018**, *98*, 115413. [[CrossRef](#)]
44. Champo, A.E.; Naumis, G.G. Metal-insulator transition in 8-*Pmmn* borophene under normal incidence of electromagnetic radiation. *Phys. Rev. B* **2019**, *99*, 035415. [[CrossRef](#)]
45. Ibarra-Sierra, V.G.; Sandoval-Santana, J.C.; Kunold, A.; Naumis, G.G. Dynamical band gap tuning in anisotropic tilted Dirac semimetals by intense elliptically polarized normal illumination and its application to 8-*Pmmn* borophene. *Phys. Rev. B* **2019**, *100*, 125302. [[CrossRef](#)]
46. Paul, G.C.; Islam, S.K.F.; Saha, A. Fingerprints of tilted Dirac cones on the RKKY exchange interaction in 8-*Pmmn* borophene. *Phys. Rev. B* **2019**, *99*, 155418. [[CrossRef](#)]
47. Zhang, S.-H.; Shao, D.-I.; Yang, W. Velocity-determined anisotropic behaviors of RKKY interaction in 8-*Pmmn* borophene. *J. Magn. Magn. Mater.* **2019**, *491*, 165631. [[CrossRef](#)]
48. Zhang, S.-H.; Yang, W. Anomalous caustics and Veselago focusing in 8-*Pmmn* borophene $p-n$ junctions with arbitrary junction directions. *New J. Phys.* **2019**, *21*, 103052. [[CrossRef](#)]
49. Gao, M.; Yan, X.-U.; Wang, J.; Lu, Z.-H.; Xiang, T. Electron-phonon coupling in a honeycomb borophene grown on Al (111) surface. *Phys. Rev. B* **2019**, *100*, 024503. [[CrossRef](#)]
50. Kapri, P.; Dey, B.; Ghosh, T.K. Valley caloritronics in a photodriven heterojunction of Dirac materials. *Phys. Rev. B* **2020**, *102*, 045417. [[CrossRef](#)]
51. Zheng, J.-I.; Lu, J.-U.; Zhai, F. Anisotropic and gate-tunable valley filtering based on 8-*Pmmn* borophene. *Phys. Rev. B* **2020**, *32*, 025205.
52. Zhou, X.-I. Anomalous Andreev reflection in an 8-*pmmn* borophene-based superconducting junction. *Phys. Rev. B* **2020**, *102*, 045132. [[CrossRef](#)]
53. Nguyen, V.H.; Charlier, J.C. Klein tunneling and electron optics in Dirac-Weyl fermion systems with tilted energy dispersion Superlattices. *Phys. Rev. B* **2018**, *97*, 235113. [[CrossRef](#)]
54. Zhang, S.-H.; Zhu, J.-I.; Yang, W.; Lin, H.-A.; Chang, K. Hidden quantum mirage by negative refraction in semiconductor P-N junctions. *Phys. Rev. B* **2016**, *94*, 085408. [[CrossRef](#)]
55. Zhang, S.-H.; Yang, W.; Peeters, F.M. Veselago focusing of anisotropic massless Dirac fermions. *Phys. Rev. B* **2018**, *97*, 205437. [[CrossRef](#)]
56. Hahn, T. *International Tables for Crystallography, Volume A*; Springer: Berlin/Heidelberg, Germany, 2005; p. 59.
57. Napitu, B.D. Photoinduced Hall effect and transport properties of irradiated 8-*Pmmn* borophene monolayer. *J. Appl. Phys.* **2020**, *128*, 039901. [[CrossRef](#)]
58. Li, H.-A.; Wang, L.; Lan, Z.-H.; Zheng, Y.-I. Generalized transfer matrix theory of electronic transport through a graphene waveguide. *Phys. Rev. B* **2009**, *79*, 155429. [[CrossRef](#)]
59. Zhang, L.B.; Chang, K.; Xie, X.-I.; Buhmann, H.; Molenkamp, L.W. Quantum tunneling through planar $p-n$ junctions in HgTe quantum wells. *New J. Phys.* **2010**, *12*, 083058. [[CrossRef](#)]
60. Zhan, T.-I.; Shi, X.; Dai, Y.Y.; Liu, X.H.; Zi, J. Transfer matrix method for optics in graphene layers. *J. Phys. Condens. Matter.* **2013**, *25*, 215301. [[CrossRef](#)]
61. Li, Z.-H.; Cao, T.; Wu, M.; Louie, S.G. Generation of Anisotropic Massless Dirac Fermions and Asymmetric Klein Tunneling in Few-Layer Black Phosphorus Superlattices. *Nano Lett.* **2017**, *17*, 2280–2286. [[CrossRef](#)]
62. Huard, B.; Sulpizio, J.A.; Stander, N.; Todd, K.; Yang, B.; Goldhaber-Gordon, D. Transport Measurements Across a Tunable Potential Barrier in Graphene. *Phys. Rev. Lett.* **2007**, *98*, 236803. [[CrossRef](#)]
63. Datta, S. *Electronic Transport in Mesoscopic Systems*; Cambridge University Press: Cambridge, UK, 1999; pp. 48–110.
64. Allain, P.E.; Fuchs, J.N. Klein tunneling in graphene: Optics with massless electrons. *Eur. Phys. J. B* **2011**, *83*, 301–317. [[CrossRef](#)]